Astron. Astrophys. 267, 265–274 (1993)

ASTRONOMY AND ASTROPHYSICS

Rotational effects on convection simulated at different latitudes

Pentti Pulkkinen[1], **Ilkka Tuominen**[2], **Axel Brandenburg**[2,3], **Åke Nordlund**[4], **Robert F. Stein**[5]

[1] Dept. of Theoretical Physics, University of Helsinki, Siltavuorenpenger 20C, SF-00170 Helsinki, Finland
[2] Observatory and Astrophysics Laboratory, University of Helsinki, Tähtitorninmäki, SF-00130 Helsinki, Finland
[3] NORDITA, Blegdamsvej 17, DK-2100 Copenhagen Ø, Denmark
[4] Copenhagen University Observatory, Øster Voldgade 40, DK-1350 Copenhagen K, Denmark
[5] Dept. of Physics and Astronomy, Michigan State University, East Lansing, MI 48824, USA

Received March 9, accepted August 8, 1992

Abstract. We simulate numerically convection inside the solar convection zone under the influence of rotation at different latitudes. The computational domain is a small rectangular box with stress-free upper and lower boundaries, and with periodicity assumed in the lateral directions. We study the transport of angular momentum, which is important for the generation of differential rotation. The sign and the latitudinal dependence of the horizontal Reynolds stress component turn out to be in good agreement with correlation measurements of sunspot proper motions and with predictions from the theory of the Λ-effect. We also investigate the other components of the Reynolds stress as well as the eddy heat flux tensor, both of which are needed in mean field models of differential rotation.

Key words: the Sun: differential rotation – convection – turbulence

1. Introduction

In the last few years computers have become efficient enough to make three-dimensional simulations of stellar convection. Although the systems which can be handled are still quite modest compared to real stellar environments, it is possible to study physically interesting aspects, such as stratification and rotation in turbulent convection. Preliminary results (Pulkkinen et al. 1991) suggest that rotational effects on convection can be studied to some extent using local models as a complement to global models of convection in spherical shells (e.g., Gilman 1977).

We briefly review some important studies in modelling convection. Hurlburt et al. (1984) used a two-dimensional simulation without rotation to study the onset of convection as well as the time-dependence of convective motions. In a second paper (1986) they included penetration of convective motions into stable layers. In these papers the importance of a sufficiently large aspect ratio (horizontal dimension/vertical dimension) of the computational domain was emphasized. If the aspect ratio was too small the solution remained time-dependent whereas an otherwise similar simulation with larger aspect ratio resulted in a steady state.

A three-dimensional model with a somewhat different setup was studied by Chan & Sofia (1986, 1989). They tested the mixing length concept and noticed that the relative pressure fluctuations were not small compared to density and temperature fluctuations, in contrast to the standard mixing length and Boussinesq approximations. However, the correlation length was found to be of the order of the pressure scale height, thus supporting one of the basic assumptions of mixing length theory.

Convection under the influence of rotation using three-dimensional simulations in a box, where the angle between the directions of gravity and rotation was varied, was addressed by Hathaway & Somerville (1983). Qualitatively different behaviour occurred at different latitudes. Near the poles rotation generally suppressed convection (smaller Nusselt number), whilst at lower latitudes there was also a regime where the Nusselt number increased with the Taylor number. This behaviour was found to be associated with a more regular flow pattern at lower latitudes allowing the convection to be more efficient there.

In this work we direct our interest towards rotational effects on convection that are relevant for the generation of differential rotation. The main transporter of average angular momentum in a rotating fluid is, apart from meridional motions, the Reynolds stress $Q_{ij} = \langle u_i' u_j' \rangle$, i.e. the correlation of fluctuations of velocity components. Nondiffusive contributions to the stress tensor result from anisotropies of turbulent convection in the presence of rotation and stratification (Rüdiger 1977). This was formulated in terms of the Λ-effect which quantifies the dependence of the Reynolds stress on rotation. The horizontal component $Q_{\theta\phi}$ has also been measured from sunspot proper motions (Ward 1965, Gilman & Howard 1984, Tuominen & Virtanen 1988, Virtanen 1989, Paternò et al. 1991).

For the numerical simulations presented in this paper we use a modification of a code by Nordlund & Stein (1989) in which time is advanced by a second-order Adams-Bashforth scheme and spatial derivatives are calculated from cubic splines. The dependent variables are $\ln \rho$, $\boldsymbol{u}$, and the internal energy $e = c_V T$. (For further details and test calculations of this version of the code see Brandenburg et al. 1990). Here we compute the Reynolds stress and the energy transport tensor from convection simulated in a box placed at different latitudes in the solar convection zone.

2. Setting up the system

We place the computational domain at some depth in the convection zone in the southern hemisphere. The vertical (z-) axis of

Send offprint requests to: Pentti Pulkkinen

the box points downward (anti-parallel to the radial direction), the x-axis points north, and the y-axis east. Since the box is small in size we may assume the angular velocity to be uniform and so omit curvature effects. It is then also natural to employ averages over both horizontal directions. The number of mesh points inside the box is $31 \times 31 \times 31$ with an aspect ratio $A = 2$ so that the mesh size in the vertical direction is half of that in the horizontal directions.

The equations to be solved and stepped in time are the equations of continuity, momentum, and energy. In addition we need an equation of state (for ideal gas) to relate the thermodynamic quantities to each other. These equations are, in a rotating frame of reference,

$$\frac{\partial \rho}{\partial t} = -\nabla \cdot (\rho \boldsymbol{u}), \tag{1}$$

$$\frac{\partial \boldsymbol{u}}{\partial t} = -\boldsymbol{u} \cdot \nabla \boldsymbol{u} - \frac{1}{\rho}\nabla p - 2\boldsymbol{\Omega} \times \boldsymbol{u} + \boldsymbol{g}_{\text{eff}} + \frac{1}{\rho}\nabla \cdot \tau, \tag{2}$$

$$\rho \frac{\partial}{\partial t}(c_V T) = -\rho \boldsymbol{u} \cdot \nabla (c_V T) - p \nabla \cdot \boldsymbol{u} + \nabla \cdot (K \nabla T) + \Phi, \tag{3}$$

$$p = \mathscr{R} \rho T. \tag{4}$$

In the equation of motion (2) the viscous tensor is defined by

$$\tau_{ij} = \mu \left(\frac{\partial u_i}{\partial x_j} + \frac{\partial u_j}{\partial x_i} - \frac{2}{3}\delta_{ij} \frac{\partial u_k}{\partial x_k} \right), \tag{5}$$

and in the energy equation (3) the viscous heat is

$$\Phi = (\tau_{ij})^2 / 2\mu. \tag{6}$$

All physical quantities are denoted with their usual symbols; ρ is density, t time, $\boldsymbol{u}$ velocity, $\boldsymbol{\Omega}$ angular velocity, $\boldsymbol{g}_{\text{eff}}$ effective gravity, p pressure, μ dynamical viscosity, T temperature, c_V specific heat at constant volume, K thermal conductivity, and $\mathscr{R}$ is the gas constant.

We assume all quantities to be periodic in the horizontal directions. The upper and lower boundaries are taken to be impenetrable and stress free, i.e. the vertical velocity component and the vertical gradient of the horizontal components vanish. These conditions ensure that mass is conserved. The heat flux at the lower boundary is assumed to be constant, thus the temperature gradient is prescribed at the lower boundary. At the upper boundary the temperature is kept constant.

The height of the box is chosen as the length unit. Thus, the z-coordinate (depth) varies from z_0 (at the top) to z_0+1 (bottom). The time unit is related to the sound travel time $\int \mathrm{d}z/c$ which in our case is 0.6. The initial state is a polytrope (see e.g. Hurlburt et al. 1984), with $T = \beta^{(0)} z$ and $\rho = \rho_0 (z/z_0)^m$, where m is the polytropic index, related to the temperature gradient $\beta^{(0)}$ by

$$m = \frac{g}{\mathscr{R}\beta^{(0)}} - 1. \tag{7}$$

According to Schwarzschild's criterion m has to satisfy: $m + 1 < \gamma/(\gamma - 1)$ for convective instability. For the ratio of the specific heats, $\gamma = c_P/c_V$, we use 5/3. Thus the condition for instability is $m < 3/2$ and we use $m = 1$ for a superadiabatic reference atmosphere. Initially, in addition to the polytropic stratification, we impose a velocity field consisting of small random perturbations. In the cases presented in this paper we used $z_0 = 2$, i.e. the density ratio χ between bottom and top is initially 1.5 and the number of pressure scale heights is $m^{-1}(m+1)\ln\chi = 0.8$.

The basic units may be scaled freely in our simulation so that, in principle, the domain may be placed at any depth in the Sun. However, because of the wide range of different time and length scales that occur in the Sun, it would be too expensive in terms of computer resources to make a model where all quantities have solar values. Therefore we have to consider a model in which we artificially bring these different time scales closer together. For our purpose the most important time scale is the rotation period which, for the Sun, is 25 days. In our model the ratio between sound travel time and rotation period is only about 50, whereas at the bottom of the solar convection zone this ratio is close to 5000 (and even larger in the upper layers). Thus, we could consider either a model which rotates 100 times faster than the Sun, or one in which the sound speed is decreased by a factor of 100. The main reason why we feel that our model may still be relevant for understanding rotational effects on convection is that the *Rossby number*, which measures the ratio between turbulent and rotational velocities, *is of order unity both in our model and at the base of the solar convection zone.*

The main difference between the Sun and a numerical model is, of course, encountered with the viscosity. The molecular viscosity inside the Sun is relatively small (~ 0.1 m^2/s) so that the Reynolds number exceeds 10^{10} from which we expect fully developed turbulence. The ratio between convective and viscous forces may be measured by the Rayleigh number

$$\mathrm{Ra} = \left(\frac{g d^4}{\kappa \nu} \frac{1}{c_p} \frac{\mathrm{d}s}{\mathrm{d}z} \right)_{z=z_m}, \tag{8}$$

where s is the specific entropy and all quantities are evaluated at $z_m = z_0 + 1/2$ for the hydrostatic reference solution. Here, $\kappa = K/c_p\rho$ is the thermal diffusivity, and $\nu = \mu/\rho$ is the kinematical viscosity. Inside the Sun, Ra exceeds 10^{20} which is far too high to be handled in computer simulations, because the Reynolds number (Re$= u_t d/\nu$, where u_t is the rms velocity) would become too large for the available resolution. In order to resolve the small scales one usually requires that the effective grid Reynolds number $u_t \Delta x/\nu$ does not significantly exceed unity. One must accept the possibility that stellar convection at such high Rayleigh numbers might be qualitatively different from modest Rayleigh number convection accessible to current computer simulations. (We recall that in laboratory convection a number of qualitative changes have been detected as the Rayleigh number is increased, cf. Castaing et al. 1989.)

The efficiency of convective energy transport relative to radiative energy transport may be measured by the Nusselt number

$$\mathrm{Nu} = \frac{F_{\text{tot}} - F_{\text{ad}}}{F^{(0)}_{\text{rad}} - F_{\text{ad}}}, \tag{9}$$

where F_{tot} is the sum of convective, radiative, kinetic, and viscous fluxes, F_{ad} is the radiative flux for an adiabatic stratification, and $F^{(0)}_{\text{rad}}$ is the radiative flux for the hydrostatic (polytropic) reference solution. In the hydrostatic state, when there are no convective motions, Nu is equal to unity. When the temperature gradient is large enough, the Rayleigh number exceeds its critical value, and Nu begins to increase.

Other dimensionless parameters that describe the system are the Taylor and Prandtl numbers,

$$\mathrm{Ta} = \frac{4\Omega^2 d^4}{\nu^2}, \qquad \mathrm{Pr} = \frac{\nu}{\kappa}. \tag{10}$$

The first one is a measure of rotation and the second is the ratio between kinematic viscosity and thermal diffusivity. In Table 1 we summarize the input parameters and the quantities derived from them. Three of the initial parameters are dimensionless numbers, and the initial temperature gradient and the polytropic index determine the instability of the layer. To change the physics of the system is possible only through changing these parameters.

Table 1. Quantities derived from Eqs. (7)-(10)

Input parameter	Quantities derived from them
Rayleigh number Ra	viscosities ν, μ
Taylor number Ta	angular velocity Ω
Prandtl number Pr	thermal diffusivity κ
polytropic index m	initial entropy grad. $ds^{(0)}/dz$
depth of top layer z_0	initial density contrast χ
latitude θ	$\boldsymbol{g} \cdot \boldsymbol{\Omega}$

The only input parameters that are varied in our simulations are the Rayleigh number and the latitude. The Taylor number is 10^4 and the Prandtl number is unity in all runs. The latitude is varied from $-90°$ (south pole) in steps of 15 degrees (or less) to the equator. We also performed some runs for the northern hemisphere and found in all cases the expected symmetry properties with respect to the equator. For the Rayleigh number we consider two values (30 000 and 60 000) allowing us to study the behaviour as the strength of convection is varied. We typically simulate about 500 time units corresponding to about 20 turnover times, long enough for the medium to mix completely.

One time step takes about 0.3 sec on a Cray X-MP and one run with typically 10^5 time steps corresponds to 8 hours of CPU time. In order to estimate the total cost this has to be multiplied by the number of runs for different values of Ra and latitude (at least 2×7).

3. Turbulent transport coefficients

3.1. Angular momentum transport

Let us write the velocity as a sum of a mean-field and a fluctuation about the mean, i.e. $\boldsymbol{u} = \langle \boldsymbol{u} \rangle + \boldsymbol{u}'$. In this section we consider spherical coordinates (r, θ, ϕ) and define mean-fields as ϕ-averages. A new term, the Reynolds stress $Q_{ij} = \langle u_i u_j \rangle$, appears in the mean-field momentum (or Reynolds) equation

$$\rho \left(\frac{\partial \langle \boldsymbol{u} \rangle}{\partial t} + \langle \boldsymbol{u} \rangle \cdot \nabla \langle \boldsymbol{u} \rangle \right) = -\nabla \cdot (\rho Q) + \rho \boldsymbol{g} - \nabla p + \nabla \cdot \langle \boldsymbol{\tau} \rangle. \quad (11)$$

Here, we have suppressed the fluctuations of pressure and density and supposed that the Reynolds rules hold (see e.g. Rüdiger 1989). For the results presented here we have checked that the difference between $\langle \rho u_i' u_j' \rangle$ and $\langle \rho \rangle \langle u_i' u_j' \rangle$ is small. This Reynolds stress is the main transporter of angular momentum (for a review see, e.g., Stix 1989). Assuming axial symmetry of the averaged quantities the equation of angular momentum transport is

$$\frac{\partial}{\partial t}(\rho r^2 \sin^2\theta \Omega) + \nabla \cdot (\rho r^2 \sin^2\theta \Omega \langle \boldsymbol{u} \rangle + \rho r \sin\theta \langle u_\phi' \boldsymbol{u}' \rangle) = 0, \quad (12)$$

where $\Omega = \langle u_\phi \rangle / r \sin\theta$ is the local angular velocity in a non-rotating frame of reference.

A traditional way to approximate this stress tensor is the so-called "Boussinesq ansatz" (not to be confused with the Boussinesq approximation), $Q_{ij} = -\nu_T (u_{i,j} + u_{j,i})$, where ν_T is an eddy viscosity. This ansatz turns out to be insufficient for two reasons. Firstly, $Q_{\theta\phi}$ is observed to be positive in the northern hemisphere (and negative in the southern hemisphere), see Ward (1965). This, however, could not be explained by the Boussinesq ansatz, which yields $Q_{\theta\phi} = -\nu_T \sin\theta \frac{\partial \Omega}{\partial \theta}$. This is negative in the northern hemisphere of the Sun, because Ω increases toward the equator and ν_T is positive. Secondly, since the Boussinesq ansatz is nothing but a diffusion term, it always tends to reduce gradients in angular velocity. Thus, if the Reynolds stress is really the source of differential rotation, some further, nondiffusive, terms are needed in the expression for Q_{ij}. It is clear that stratification will always give a preferred direction to the turbulence so that it becomes anisotropic. Such an anisotropic turbulence may give additional contributions to Q_{ij} which are proportional to Ω itself (and not to its gradient) and thus do not vanish – even for uniform rotation. This was formulated by Rüdiger (1977, 1980) who introduced the theory of the Λ-effect, which has some resemblance to the theory of the α-effect in mean-field electrodynamics (Krause & Rädler 1980). The Reynolds stress is expanded as

$$Q_{ij} = \Lambda_{ijk} \Omega_k - N_{ijkl} \partial \langle u_k \rangle / \partial x_l + \ldots, \quad (13)$$

where higher derivative terms may be ignored if there is a separation of scales (e.g. Rüdiger 1989). The Boussinesq ansatz corresponds to $N_{ijkl} = \nu_T (\delta_{ik}\delta_{jl} + \delta_{jk}\delta_{il})$. The tensor Λ_{ijk} is symmetric in i and j and can therefore not be isotropic, because it would vanish otherwise. The two cross-correlations which enter in Eq. (12) may explicitly be written as

$$\frac{Q_{r\phi}}{\nu_T} = \left(-\frac{r}{\Omega} \frac{\partial \Omega}{\partial r} + V^{(0)} + V^{(1)} \sin^2\theta + V^{(2)} \sin^4\theta \right) \sin\theta \Omega, \quad (14)$$

$$\frac{Q_{\theta\phi}}{\nu_T} = \left(-\frac{1}{\Omega} \frac{\partial \Omega}{\partial \theta} + H^{(1)} \cos\theta \sin\theta + H^{(2)} \cos\theta \sin^3\theta \right) \sin\theta \Omega. \quad (15)$$

Here, the latitudinal dependence of the coefficients in the Λ-tensor has been expressed in powers of $\sin^2\theta$; for further details see Rüdiger (1980).

In principle, the tensor N_{ijkl} may also be anisotropic; e.g. Kichatinov (1986). As pointed out by Rüdiger & Tuominen (1987), the concept of anisotropic viscosity (e.g. Kippenhahn 1963) corresponds to the Λ-effect with nonvanishing $V^{(0)}$. Thus, radial differential rotation may be generated via the $Q_{r\phi}$-term, but $Q_{\theta\phi}$ would still remain negative – in disagreement with observations.

Equation (15) plays a particularly important role, because both $Q_{\theta\phi}$ and $\partial\Omega/\partial\theta$ have been observed. The solar surface rotation rate is often written in the form $\Omega = A + B\cos^2\theta + C\cos^4\theta$. Using this in (15) we obtain

$$Q_{\theta\phi} = \nu_T \Omega_\bullet (w_1 + w_2 \sin^2\theta) \cos\theta \sin^2\theta, \quad (16)$$

where

$$w_1 = H^{(1)} + 2(B + 2C)/\Omega_\bullet, \quad (17)$$

$$w_2 = H^{(2)} - H^{(1)}(B + 2C)/\Omega_\bullet - 4C/\Omega_\bullet, \quad (18)$$

and $\Omega_\bullet = A + B + C$ is the rotation rate at the poles. This form for $Q_{\theta\phi}$ is useful for comparing results from our simulations

with observations at the solar surface. Below we use solar values $B/\Omega_\odot = -0.17$ and $C/\Omega_\odot = -0.23$ and compare mainly with results obtained by Virtanen (1989), who finds the values $w_1 = 1.0$ and $w_2 = 5.6$. It should be noted that the latitudinal dependence of Ω and the Λ-terms might be more complicated, but for the present purpose the above representation seems sufficient.

3.2. Energy transport

The averaged equation for the energy transport is

$$\rho c_P \left(\frac{\partial \langle T \rangle}{\partial t} + \langle \boldsymbol{u} \rangle \cdot \nabla \langle T \rangle \right) = -\nabla \cdot (\rho c_P \langle \boldsymbol{u}' T' \rangle) - p \nabla \cdot \langle \boldsymbol{u} \rangle + \nabla \cdot (K \nabla \langle T \rangle) + \langle \Phi \rangle, \quad (19)$$

where to the simplest approximation the turbulent heat flux $\langle \boldsymbol{u}' T' \rangle$ may be written as

$$\langle u_i' T' \rangle = \chi_{ij} \beta_j, \quad (20)$$

where $\boldsymbol{\beta} = -(\nabla T - \boldsymbol{g}_{\rm eff}/c_P)$ is the superadiabatic temperature gradient. Eqs. (19) and (20) are only an approximation in that certain correlations involving density fluctuations have been neglected. This is consistent with mixing length arguments (Rüdiger 1989), but cannot be justified for strongly compressible flows. In our runs the stratification is weak and this approximation therefore appropriate.

The eddy heat flux tensor is written in the form (only radial and meridional components)

$$\frac{\chi_{ij}}{\chi_T} = \begin{pmatrix} 1 & 0 \\ 0 & 1 \end{pmatrix} - \begin{pmatrix} VV^{(1)} \sin^2\theta + VV^{(2)} \sin^4\theta & ;\ldots \\ HV^{(1)} \sin\theta \cos\theta + HV^{(2)} \sin^3\theta \cos\theta & ;\ldots \end{pmatrix} \quad (21)$$

(Tuominen & Rüdiger 1989), where χ_T is the (isotropic) eddy conductivity, and ... stands for further components which describe the flux due to the β_θ component (which vanishes in our idealized simulation with periodic boundary conditions in the horizontal directions).

4. Results

4.1. Summary of the computations

Before we present the results for the Reynolds stress and eddy heat flux tensor we first present some general properties of our simulations.

In Table 2 we give a summary of various quantities derived from the simulations for Ra=30 000 and 60 000. All the values are spatial and temporal averages, except those quantities where a maximum value is given. As a general trend, the Nusselt number, as well as the maximum Reynolds and Mach numbers (Ma= u_t/c, where c is the local sound speed) increase from the pole to the equator which indicates that convection is stronger in the equatorial regions. For Ra=60 000 the Nusselt number shows a minimum at 45°. This is in agreement with results of Gilman (1977) who finds that convection in equatorial regions is most favoured and that polar regions are favoured next, whilst middle latitudes are not favoured. Both at the equator and at the poles pressure gradients can balance the Coriolis force and can thus help neutralize the stabilizing effect of rotation. However, at the poles, where the Coriolis force has only horizontal components, strong swirling motions are produced which increase the dissipation there. Similar results have been obtained by Busse & Cuong (1977), who associate this behaviour with the different convection pattern at high and low latitudes.

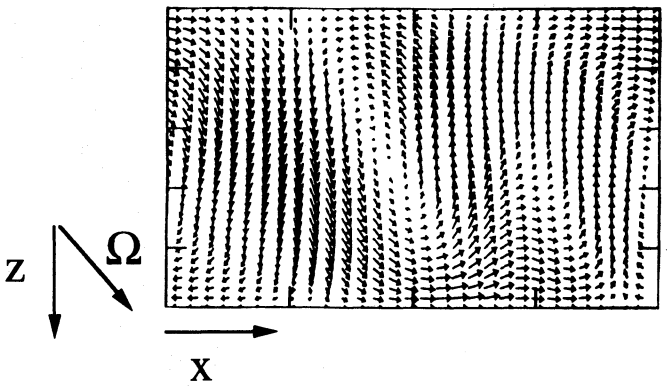

Fig. 1. A snapshot from a simulation with Ra=30 000 and latitude −45°. Note the tilt of the cell structures parallel to the direction of Ω

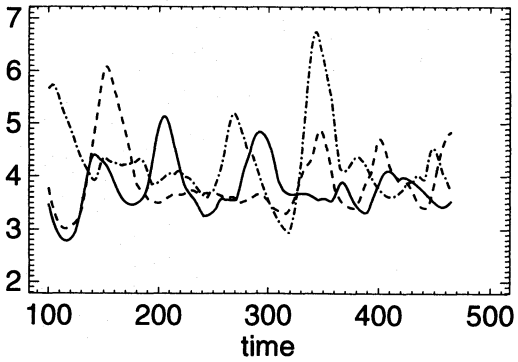

Fig. 2. A time sequence of the Nusselt number at latitudes −30° (dash-dotted), −45° (solid), and −60° (dashed) for Ra=60 000

From the Nusselt numbers obtained for the two values of Ra we may also estimate the critical Rayleigh number, Ra_c, plotting lnNu vs. lnRa and extrapolating a straight line to lnNu=0 which corresponds to $\mathrm{Ra}=\mathrm{Ra}_c$ (last row in Table 2). This extrapolation becomes obviously inaccurate for small critical Rayleigh numbers. We find that Ra_c is smallest at the equator and largest at the poles. There is no tendency for Ra_c to increase from the poles to middle latitudes, but rather that Ra_c has a local minimum at 45°. This is unexpected and may be due to either non-linear dependence of Nu on Ra or transients and uncertainties arising from relatively strong temporal fluctuations in the time sequence of the Nusselt number; see Fig. 2 where we have plotted the evolution of Nu for Ra=60 000 at three different latitudes.

Note that the maximum Reynolds and Mach numbers typically increase with Ra, except for the equator, where high peak velocities occurred for Ra=30 000.

The entropy difference between top and bottom, $\Delta\langle s \rangle$, decreases slightly from the pole to the equator meaning that the layer becomes more adiabatic towards the equator. This is consistent with convection being more efficient there. The kinetic flux points downwards (i.e. $F_{\rm kin} < 0$), because the downward directed flow is more concentrated. Both $F_{\rm conv}$ and $|F_{\rm kin}|$ increase toward the equator.

Table 2. Various quantities obtained from the simulations. In the upper row of each quantity Ra is 30000 and in the lower one it is 60000. The critical Rayleigh number for the onset of convection is given in the last row

latitude	−90°	−75°	−60°	−45°	−30°	−15°	0°
Nu	2.69	2.68	2.69	2.87	2.90	3.25	3.98
	3.68	3.65	3.56	3.39	3.80	4.06	4.70
Re(max)	18	19	20	21	21	23	40
	20	20	21	21	22	27	37
Ma(max)	0.028	0.029	0.031	0.033	0.033	0.036	0.062
	0.030	0.031	0.033	0.033	0.035	0.042	0.056
$\Delta\langle s\rangle$	0.086	0.087	0.087	0.086	0.085	0.082	0.076
	0.079	0.079	0.080	0.080	0.078	0.076	0.074
$F_{\rm rad}/F_{\rm tot}$	0.83	0.83	0.82	0.81	0.81	0.81	0.79
	0.81	0.81	0.81	0.81	0.80	0.80	0.79
$F_{\rm conv}/F_{\rm tot}$	0.18	0.17	0.18	0.19	0.19	0.20	0.22
	0.19	0.20	0.19	0.20	0.21	0.21	0.23
$F_{\rm kin}/F_{\rm tot}$	−0.002	−0.000	−0.002	−0.005	−0.003	−0.007	−0.008
	−0.003	−0.003	−0.003	−0.007	−0.009	−0.011	−0.021
Ra_c	3330	3270	2540	600 (?)	1970	1030	260

The orientation of convection elements is somewhat tilted against the vertical and the structures seem to line up with the rotation vector; see Fig. 1. This is expected if the Taylor number is sufficiently large (Taylor-Proudman theorem, e.g. Chandrasekhar 1961).

We now consider the latitudinal dependence of the degree of anisotropy of the flow. This may be quantified by measuring the relative magnitudes of $\langle u_\theta^2\rangle$, $\langle u_\phi^2\rangle$, and $\langle u_r^2\rangle$; see Fig. 3 where the average has been taken also in the radial direction. Note that $\langle u_\phi^2\rangle$ increases more strongly toward the equator than $\langle u_r^2\rangle$ and $\langle u_\theta^2\rangle$ such that between latitudes 0° and 60° $\langle u_\phi^2\rangle$ is larger than both $\langle u_\theta^2\rangle$ and $\langle u_r^2\rangle$, whereas at higher latitudes these components are more or less equal. If we consider only horizontal averages then we find that they vary strongly with depth. In Fig. 4 we give the latitudinal dependence of the quantity

$$W(r,\phi) \equiv \frac{\langle u_r^2\rangle - \langle u_\phi^2\rangle}{\langle u_r^2\rangle + \langle u_\phi^2\rangle} \tag{22}$$

at depths $z = 2.13$ and $z = 2.63$ as well as its average over all depths In the upper layers the velocity fluctuations in the ϕ-direction dominate and the slope of this curve retains its sign. In the mid-layer ($z = 2.63$) the flow in the radial direction dominates – as expected (cf. Fig 10 in Brandenburg et al. 1990), and is smallest at mid-latitudes indicating a possible change of anisotropy there.

Before we proceed to compute Reynolds stress components and heat fluxes we need to discuss the statistical error involved in the computation of averages of a simulated time sequence. As a typical example of such a time sequence we show in Fig. 5 the evolution of $Q_{\theta\phi}$ at −60° close to the upper layer of the box. As with all time dependent quantities, we exclude the first 100 time units in order to minimize the influence of the initial transient phase. The duration of the runs was limited by economical aspects. In Fig. 5 we show also the average value and the standard deviation $s = \sqrt{\overline{x^2} - \overline{x}^2}$ denoting the width of the fluctuations. We could estimate the statistical error of the average value by using the mean error of the mean $\sigma = s/\sqrt{n}$, where n is the number

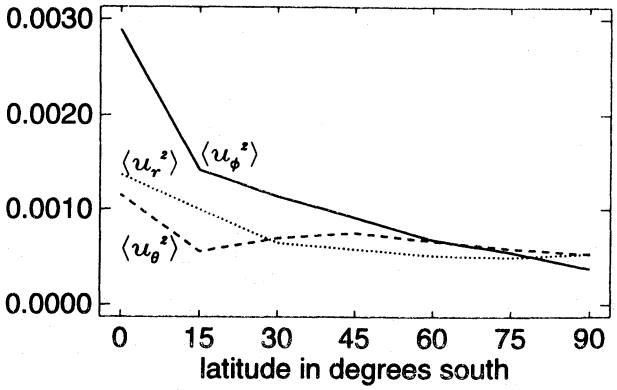

Fig. 3. Latitudinal dependence of the radially and horizontally averaged components of the turbulent velocity

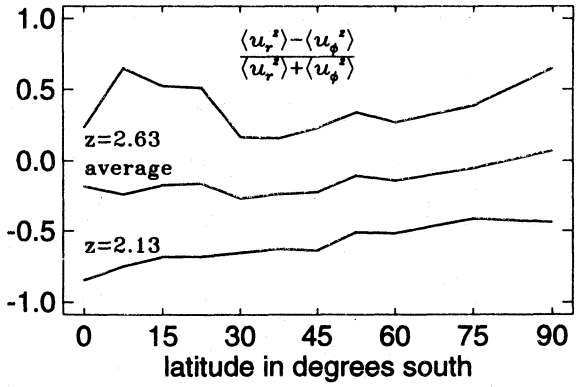

Fig. 4. Latitudinal dependence of the relative magnitude $W(r,\phi)$ (eq. 22) at depths 2.13 and 2.63. In addition the average over all depths is shown.

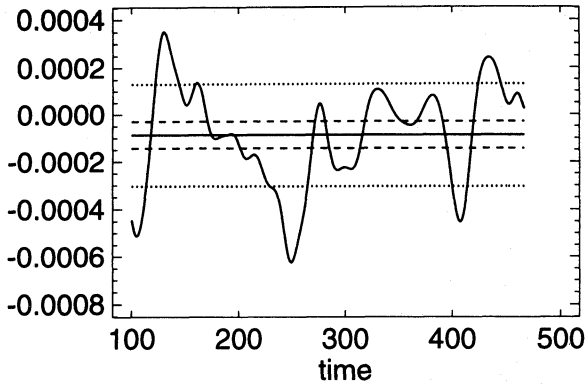

Fig. 5. A time sequence of $Q_{\theta\phi}$ at $-60°$ close to the upper layer of the box. The solid line in the middle is the average value whilst the inner lines (dashed) denote the modified mean error of the mean where the non-zero autocorrelation time between successive time steps has been taken into account. The outer lines (dotted) show the standard deviation, i.e. the width of the fluctuations

of data points. However, due to the numerical integration of the equations the successive data points are not independent of each other. Therefore, we have to take into account the *autocorrelation* of the time sequence vector $\boldsymbol{x}$. This autocorrelation is computed with the quantity

$$\Gamma_q = \left(\sum_{i=1}^{n-q} x_i x_{i+q} - \frac{1}{n-q} \sum_{j=1}^{n-q} \sum_{k=q+1}^{n} x_j x_k \right) \frac{1}{(n-q)\sigma},$$
$$q = 1, \ldots, q_c. \qquad (23)$$

The index q_c is reached when Γ_q becomes smaller than some fixed (small positive) value. Then there is no correlation between data points x_i and x_{i+q_c}. Finally, the error is defined as $\xi = (1+ \mid \sum_{q=1}^{q_c} \Gamma_q \mid)\sigma$, so it is larger than the mean error of the mean. Should the data points be distributed randomly, the autocorrelation would vanish and we would get just the mean error of the mean. For a reference, see e.g. Priestley (1981). In the following plots the error bars always indicate this modified error.

4.2. The Reynolds stress

The Reynolds stress may be computed directly from simulations. With $u_i' = u_i - \langle u_i \rangle$, we obtain

$$\langle u_i' u_j' \rangle = \langle (u_i - \langle u_i \rangle)(u_j - \langle u_j \rangle) \rangle = \langle u_i u_j \rangle - \langle u_i \rangle \langle u_j \rangle. \qquad (24)$$

In Fig. 6 the horizontal cross-correlation $Q_{\theta\phi}$ is plotted at depth $z = 2.97$ (close to the lower boundary) for a run with Ra=30 000. In upper layers a similar shape as in the lower ones is obtained, but in the middle layers $Q_{\theta\phi}$ is small and may change sign. However, the average over the vertical direction of $Q_{\theta\phi}$ is negative throughout the southern convection zone. The latitudinal dependence of $Q_{\theta\phi}$ is qualitatively the same when we adopt total averages over the box instead of horizontal averages.

The behaviour of $Q_{\theta\phi}$ with Ra=60 000 is found to be quite similar to the one with smaller Rayleigh number (cf. Fig. 8). For higher Rayleigh numbers, however, the adopted resolution may become insufficient and therefore we focused mostly on the results for Ra=30 000.

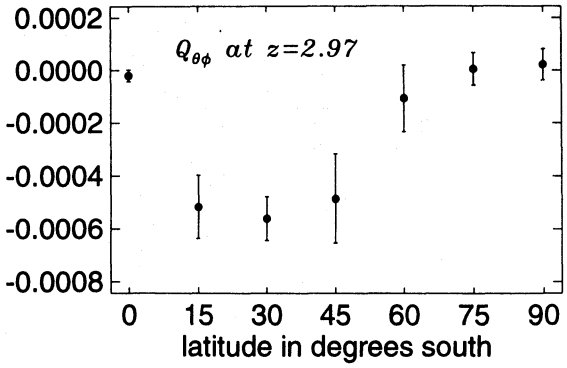

Fig. 6. The simulated horizontal Reynolds stress $Q_{\theta\phi}$ at the depth $z = 2.97$ with Ra=30 000. The error bars indicate the time-dependent data taking the autocorrelation time of the successive time steps into account (cf. Fig. 5)

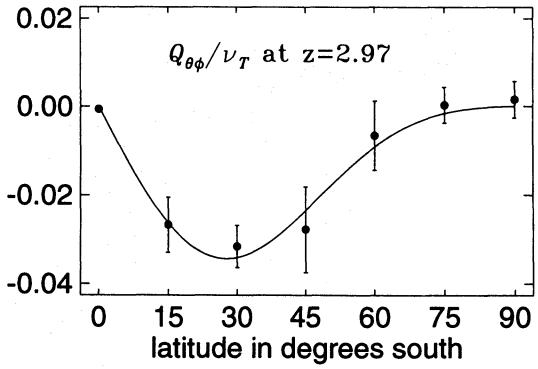

Fig. 7. The fit for $Q_{\theta\phi}/\nu_T$ at depth $z = 2.97$ with Ra= 30 000, where ν_T is latitude dependent

Simulations performed at different latitudes for the same Rayleigh number are not necessarily directly comparable with each other because the critical Rayleigh numbers for the onset of convection differ (see the last row in Table 2) and therefore the strength of convection is different. This gives rise to different values for the effective viscosity $\nu_T \approx \frac{1}{3}\langle u_t \rangle d$, which then also depends on latitude. Here we made the crude assumption that the mixing length is equal to the depth of the box corresponding to about 0.8 pressure scale heights. In Fig. 7 we have made a least-square fit for the normalized values $Q_{\theta\phi}/\nu_T$ using Eq. (16).

In Table 3 we give the w-coefficients of various sources. The Boussinesq ansatz gives a negative sign for w_1 if solar values are inserted in Eqs. (17) and (18), but using $H^{(1)} = H^{(2)} = 0$. The study by Ward (1965) is based on the Greenwich sunspot proper motions between years 1925-1954. The result by Virtanen (1989) is a fit to the Greenwich data until 1976. From these works we may conclude that the horizontal correlation $Q_{\theta\phi}$ has been observed to have positive sign in the northern hemisphere and to change its sign at the equator. The values of our simulations are from fits to the data of Figs. 6 and 7, in the first of which we have a constant eddy viscosity and in the second one it is latitude-dependent. The values in the last two rows are based on work by Tuominen & Rüdiger (1989). They used the observations as constraints in a model for differential rotation and derived the $H^{(\ell)}$ (and $V^{(\ell)}$) coefficients inside the convection zone through inversion. From these models we determined the coefficients w_1

Table 3. Comparison of the coefficients w_1 and w_2 derived from different sources (see text)

	w_1	w_2
Boussinesq-ansatz	−1.1	+0.1
Ward (1965)	+2	0
Virtanen (1989)	+1.0	+5.6
This work; v_T=const.=$v_T(45°)$	+0.11	+1.2
This work; $v_T = v_T(\theta)$	+0.18	+1.0
Tuominen & Rüdiger (O)	+6.2	+1.3
Tuominen & Rüdiger (S)	+4.5	+2.9

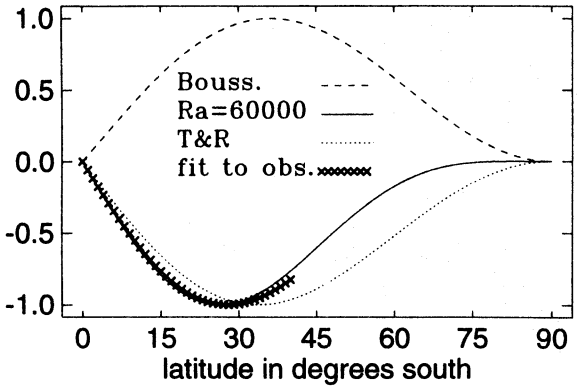

Fig. 8. The horizontal Reynolds stress $Q_{\theta\phi}$ at $z = 2.97$ obtained from our simulations with Rayleigh number 60 000 (solid line) compared with the standard Boussinesq-ansatz (dashed line), a fit (crosses) to observations by Virtanen, and results of a theoretical model by Tuominen & Rüdiger with two (dotted line). Note that the crosses cover only latitudes 0-40°. All the profiles have been scaled so that the absolute value of the extremum is equal to unity

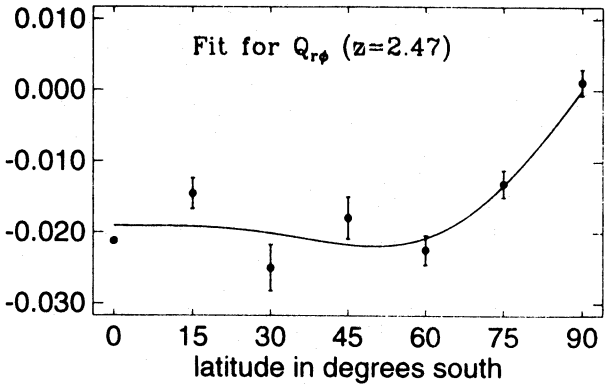

Fig. 9. The fit for $Q_{r\phi}$ at depth $z = 2.47$

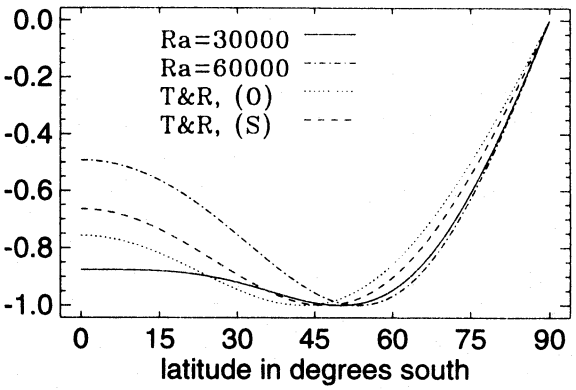

Fig. 10. The component $Q_{r\phi}$ of the Reynolds stress obtained from simulations with Rayleigh number 30 000 (solid line) and 60 000 (dash-dotted) compared with results by Tuominen & Rüdiger with two differential rotation profiles (O) (dotted line) and (S) (dashed line). All the profiles have been scaled with their absolute maximum

and w_2 *at the bottom* of the convection zone by including the observed differential rotation profile (O) into Eq. (16). The values in the last row were based on an additional constraint using the differential rotation profile at the bottom of the convection zone, as estimated by Stenflo (1989) who used magnetic tracers. In Fig. 8 we compare the various profiles for $Q_{\theta\phi}/v_T$, which are normalized to have an extremum of ± 1. This normalization allows a better comparison of the shape of the different profiles than is possible from Table 3. According to the observations the extremum of the correlation $Q_{\theta\phi}$ occurs at a latitude 25-30°; the simulations show the same behaviour. The extremum of the correlation of the work by Tuominen & Rüdiger is at higher latitudes than in our simulations, about 30-35°.

We now consider the correlation $Q_{r\phi}$. Because of the stress-free boundary conditions of our model, $Q_{r\phi}$ vanishes at the upper and lower boundaries. Therefore we choose to evaluate $Q_{r\phi}$ in the mid-layer of the box. Fig. 9 shows a fit of $Q_{r\phi}$ to Eq. (14) again using a latitude dependent profile for v_T. $Q_{r\phi}$ is clearly negative and maintains its sign also in the northern hemisphere, because the radial and latitudinal flows do not change their sign at the equator. In this fit we have neglected $\partial\Omega/\partial r$. However, we note that the fit obtained may be sensitive to this term. We estimated $\partial\Omega/\partial r$ by measuring $\partial\langle u_\phi\rangle/\partial r$ from our simulations and found that $\partial\Omega/\partial r > 0$ at high latitudes and $\partial\Omega/\partial r < 0$ at low latitudes. At higher latitudes the effect of this gradient is small, only a few per cent of the other terms but closer to the equator the angular velocity gradient begins to dominate. If we take these gradients into account we find significant deviations from the fit in Fig. 9, especially at lower latitudes where the resulting shear is large. However, this large shear may be an artifact of the local model and may be absent in a more realistic setup where the influence of boundary conditions is reduced. Helioseismological observations also suggest that $\partial\Omega/\partial r$ is small inside the convection zone, and it seems therefore sensible to neglect this term. For example Dziembowski et al. (1989) estimate for the change of the angular velocity in the radial direction to be about 10% at the equator and less elsewhere.

In Fig. 10 we compare the fits obtained from runs with two different Rayleigh numbers with the profile O and S used by Tuominen & Rüdiger. All these profiles have in common that $V^{(0)}$ and $V^{(2)}$ are negative and $V^{(1)}$ is positive. Our simulations show that $Q_{r\phi}$ is negative and possibly increasing in magnitude between the equator and 55° latitude. The two solutions used by Tuominen & Rüdiger (1989) for the different angular velocity profiles (O) and (S) also give a negative value for the correlation *in the middle* of the convection zone. At a radius of about 0.8 solar radii the sign of $Q_{r\phi}$ changes in their model and is positive

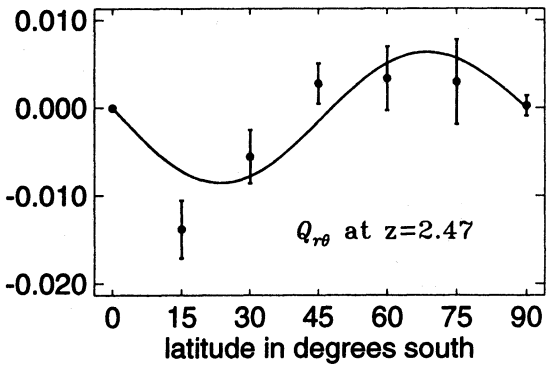

Fig. 11. The fit for $Q_{r\theta}$ at depth $z = 2.47$

at the bottom of the convection zone suggesting a change of the dominant direction of turbulence at the lower parts.

Finally we consider the correlation $Q_{r\theta}$. In the past not much attention has been paid to this quantity, because it does not directly enter in the angular momentum equation (12). However, $Q_{r\theta}$ may be important for enhancing or quenching meridional flows. $Q_{r\theta}$ must be proportional to $\cos\theta \sin\theta$ and, in analogy with Eqs. (14) and (15), we write

$$Q_{r\theta} = v_t \cos\theta \sin\theta (M^{(1)} + M^{(2)} \sin^2\theta). \quad (25)$$

The corresponding fit is shown in Fig. 11 and the coefficients are $M^{(1)} = -0.03$ and $M^{(2)} = 0.06$. Again, we used the same latitude dependent estimate for v_t as for the previous fits. Most likely higher order terms are necessary, but for the present purpose it is sufficient to note that our simulations indicate negative values of $Q_{r\theta}$ immediately south from the equator and perhaps positive values close to the southern pole.

4.3. The energy transport tensor

We compute the convective flux and calculate the eddy heat transport tensor χ_{ij} using Eq. (20). Since the mid-layers of the box are almost adiabatic β_r is close to zero and $\chi_{rr} = \langle u_r' T' \rangle / \beta_r$ is not well defined, whilst close to the upper and lower boundaries the radial heat flux approaches zero. Therefore, it is convenient to evaluate χ_{ij} some short distance away from the top and bottom boundaries. We choose the two depths, $z = 2.13$ and $z = 2.30$, and find that χ_{rr} behaves differently in these two layers. Again, we use a latitude-dependent eddy diffusivity χ_T in accordance with Eq. (21), assuming $\chi_T = \nu_T$. In Fig. 12 we give a plot of the latitudinal dependence of χ_{rr} with its fit to Eq. (21) for these two values of z. Note that close to the upper boundary (first panel) χ_{rr} has a maximum close to the pole whereas at the deeper layer (second panel) a maximum is reached in the equatorial region. The latter result agrees with the fact that the Nusselt number is larger at the equator; see Table 2. However, although $\langle u_r' T' \rangle$ is largest at the equator in both cases, a different behaviour of β_r with latitude at the two depths changes the behaviour of χ_{rr}. At $z = 2.13$ the superadiabaticity is smallest at the equator which is a result from the more efficient convection there (cf. Table 2). We see that χ_{rr} is positive everywhere which is to be expected, because β_r as well as the convective flux are directed upwards in the convection zone.

Figure 13 shows the results of simulations for $\chi_{\theta r}$. The fit does not apply too well for the data ($z = 2.13$) which show

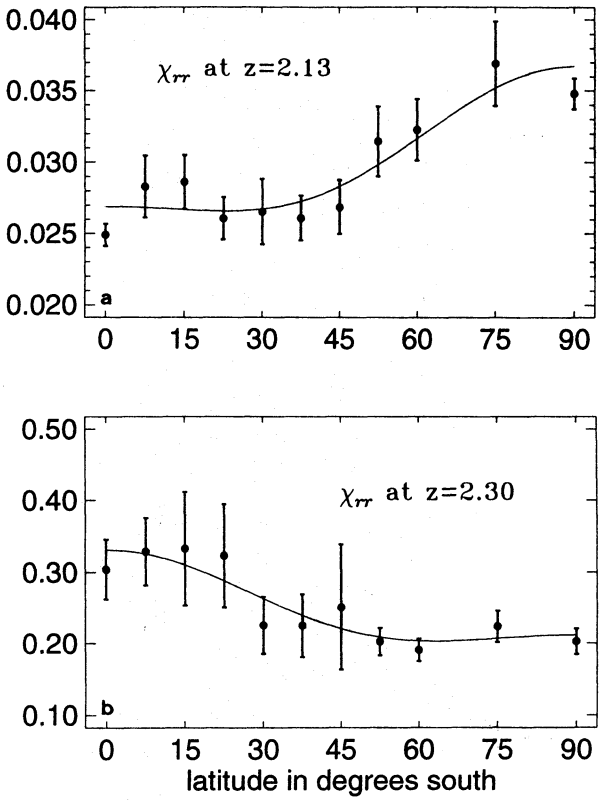

Fig. 12. The fit for χ_{rr} at depths $z = 2.13$ (upper panel) and $z = 2.30$ (lower panel)

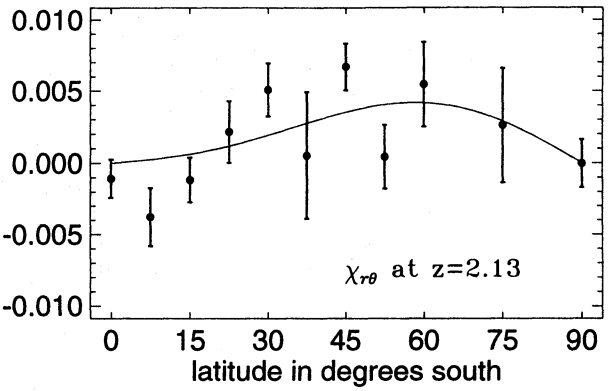

Fig. 13. The fit for $\chi_{r\theta}$ at depth $z = 2.13$

strong scatter about zero indicating that this result comes largely from random fluctuations. Away from the equatorial regions $\chi_{\theta r}$ is mainly positive and has a maximum near 45°. For the coefficients of the eddy heat flux we get the values shown in Table 4.

Finally, we note that we also performed a few simulations for a domain with aspect ratio $A = 4$ using $63 \times 63 \times 31$ grid points. The results for the Reynolds stress and the heat flux tensor are quite similar to those obtained for smaller aspect ratio, but we typically find fluctuations larger than in the case with smaller aspect ratio.

Table 4. The coefficients for the eddy heat flux tensor

	$VV^{(1)}$	$VV^{(2)}$	$HV^{(1)}$	$HV^{(2)}$
$z = 2.13$	0.65	−0.38	0.33	−0.29
$z = 2.30$	0.39	−0.95	0.36	−0.52

5. Discussion

The Reynolds stress results are important for at least two reasons. First, they prove that the "Boussinesq-ansatz" is inadequate to explain the observed and simulated results. Secondly, they show that a global spherical model might not be required for understanding the rotational influence on stellar convection. A global model has the advantage that one can directly measure the resulting differential rotation in addition to the Reynolds stresses (see e.g. Gilman, 1977). Also meridional flows, which can only be obtained from a global model, might have some influence on the Reynolds stress. However, in a global model it is more difficult to properly resolve the narrow downdrafts that occur in strongly stratified convection, and that might be crucial for the turbulent transport properties (Spruit et al. 1989, Cattaneo et al. 1991). A further uncertainty of our approach is how to compare the different runs obtained for various latitudes, in particular the estimate $\nu_T = \frac{1}{3} u_t d$ for the latitude dependent turbulent diffusivity may be too simple.

We observe a change in the degree of anisotropy as we go from the pole toward the equator. At low latitudes the (radial and horizontal) average velocity fluctuations in the ϕ-direction tend to dominate over those in the r-direction, whilst close to the poles the velocity fluctuations in the three directions are of similar order of magnitude. From this we may obtain an independent estimate for the vertical Reynolds stress versus latitude. Its sign would lead to positive values of $\partial\Omega/\partial r$ at lower latitudes and to a negative one at higher latitudes. This would be in qualitative agreement with current results of helioseismology. However, this result is based on averages taken over the entire box. Using only horizontal averages instead we find that in the middle of the layer the radial velocity fluctuations always dominate over the other two. This contributes to the negative sign of $Q_{r\phi}$ and would cause a negative value of $\partial\Omega/\partial r$ in middle layers.

Investigations of differential rotation based on mean-field models have the problem that there is a large number of ill-known turbulent transport coefficients (Λ-effect and diffusion coefficients). So far these coefficients have often been determined using first order smoothing, even though it was clear that this is not well justified under solar conditions where the correlation time is long. The present approach to determine turbulent transport coefficients from direct simulations may therefore be a useful alternative to first order smoothing methods. Apart from the $Q_{r\phi}$ and $Q_{\theta\phi}$ components of the Reynolds stress tensor we have also estimated the $Q_{r\theta}$ component, which has often been neglected in previous studies, but may be important for understanding the relatively weak meridional flow in the Sun.

Finally, we should point out that the differential rotation in our simulation cannot directly be applied to the global differential rotation of the Sun. For this purpose a global model is needed where artificial boundaries are absent. The assumption of impenetrable upper and lower boundaries in our model will also have a strong influence on the quantitative results for the various correlations. Such restrictive conditions could be somewhat relaxed by embedding the unstably stratified region between stably stratified overshoot layers. Preliminary investigations indicate that several conclusions might be affected by that.

Acknowledgements. P.P. is indebted to Nordita for their hospitality during his visit. The computations were carried out on the Cray X-MP/432 of the Centre for Scientific Computing, Espoo, Finland. R.F.S. was funded by NASA grant NAGW-1695, while Å.N. was supported by the Danish Natural Science Research Council and the Danish Space Board.

References

Brandenburg, A., Nordlund, Å., Pulkkinen, P., Stein, R. F., Tuominen, I.: 1990, *Astron. Astrophys.* **232**, 277
Busse, F. H., Cuong, P. G.: 1977, *Geophys. Astrophys. Fluid Dyn.* **8**, 17
Castaing, B., Gunaratne, G., Heslot, F., Kadanoff, L., Libchaber, A., Thomae, S., Wu, X.-Z., Zaleski, S., Zanetti, G.: 1989, *J. Fluid Mech.* **204**, 1
Cattaneo, F., Brummell, N. H., Toomre, J., Malagoli, A., Hurlburt, N. E.: 1991, *Astrophys. J.* **370**, 282
Chan, K. L., Sofia, S.: 1986, *Astrophys. J.* **307**, 222
Chan, K.L., Sofia, S.: 1989, *Astrophys. J.* **336**, 1022
Chandrasekhar, S.: 1961, *Hydrodynamic and Hydromagnetic Stability*, Clarendon Press, Oxford
Dziembowski, W.A., Goode, P.R., Libbrecht, K.G.: 1989, *Astrophys. J.* **337**, L53
Gilman, P. A.: 1977, *Geophys. Astrophys. Fluid Dyn.* **8**, 93
Gilman, P. A., Howard, R.: 1984, Solar Phys, 93, 171
Hathaway, D. H., Somerville, R. C. J.: 1983, *J. Fluid Mech.* **126**, 75
Hurlburt, N. E., Toomre, J., Massaguer, J. M.: 1984, *Astrophys. J.* **282**, 557
Hurlburt, N. E., Toomre, J., Massaguer, J. M.: 1986, *Astrophys. J.* **311**, 563
Kichatinov, L.L.: 1986, *Geophys. Astrophys. Fluid Dyn.* **35**, 93
Kippenhahn, R.: 1963, *Astrophys. J.* **137**, 664
Krause, F. & Rädler, K.-H.: 1980, *Mean-field magnetohydrodynamics and dynamo theory*, Akademie-Verlag, Berlin
Nordlund, Å., Stein, R. F.: 1989, in *Solar and Stellar Granulation*, eds. R. Rutten and G. Severino, Kluwer Acad. Publ.
Paternò, L., Spadaro, D., Zappala, R. A., Zuccarello, F.: 1991, *Astron. Astrophys.* **252**, 337
Priestley, M.B.: 1981, *Spectral Analysis and Time Series*, Academic Press, London
Pulkkinen, P., Tuominen. I., Brandenburg. A., Nordlund, Å., Stein, R.F.: 1991, in *The Sun and cool stars: activity, magnetism, dynamos*, eds. I. Tuominen, D. Moss & G. Rüdiger, Lecture Notes in Physics **380**, Springer-Verlag, p. 98
Rüdiger, G.: 1977, *Astron. Nachr.* **298**, 245
Rüdiger, G.: 1980, *Geophys. Astrophys. Fluid Dyn.* **16**, 239
Rüdiger, G.: 1989 *Differential Rotation and Stellar Convection: Sun and Solar-type Stars*, Akademie-Verlag Berlin & Gordon and Breach, New York
Rüdiger, G., Tuominen, I.: 1987, in *The Internal Solar Angular Velocity*, eds. B.R. Durney and S. Sofia, p. 361
Spruit, H. C., Nordlund, Å, Title, A. M.: 1990, *Ann. Rev. Astron. Astrophys.* **28**, 263
Stenflo, J.: 1989, *Astron. Astrophys.* **210**, 403

Stix, M.: 1989, *The Sun: An introduction*, Springer-Verlag, Berlin Heidelberg
Tuominen, I., Rüdiger, G.: 1989, *Astron. Astrophys.* **217**, 217
Tuominen, I., Virtanen, H.: 1988, *Adv. Space Res.* **8**, (7)141
Virtanen, H.: 1989, Licentiate thesis, University of Helsinki
Ward, F.: 1965, *Astrophys. J.* **141**, 534

This article was processed by the author using Springer-Verlag LaTeX A&A style file 1990.